

Compact star clusters of the LMC H II region N11 C^{*}

Mohammad Heydari-Malayeri¹, Pierre Royer^{**,2}, Gregor Rauw^{***,2}, and Nolan R. Walborn³

¹ DEMIRM, Observatoire de Paris, 61 Avenue de l'Observatoire, 75014 Paris, France

² Université de Liège, Institut d'Astrophysique et de Géophysique, 5 Avenue de Cointe, 4000 Liège, Belgium

³ Space Telescope Science Institute, 3700 San Martin Drive, Baltimore, MD 21218, USA

Received 4 April 2000 / Accepted 20 July 2000

Abstract. Based on imaging and spectroscopy obtained at the ESO NTT telescope and using an efficient image analysis algorithm, we study the core of the LMC OB association LH 13, particularly the two compact stellar clusters Sk-66°41 and HNT in the H II region N 11C. We resolve Sk-66°41 into 15 components and for the first time the HNT cluster into 70 stars, and derive photometry for the members. Moreover, from medium resolution spectroscopy we determine the spectral types for sixteen stars in N 11C. We compare the color-magnitude diagrams of the clusters with that of the field stars and discuss the cluster ages. With an age of ~ 100 Myr, the HNT cluster appears significantly older than the very young (≤ 5 Myr) Sk-66°41 starburst. We suggest that most of the 'field' O-stars in the core of N 11C have actually been ejected from Sk-66°41 through dynamical interactions in the compact cluster. The properties of the Sk-66°41 and HNT clusters suggest that we are viewing different star formation regions lying at different distances along the same line of sight.

Key words: stars: early-type – ISM: H II regions – ISM: individual objects: N 11C – galaxies: Magellanic Clouds

1. Introduction

The giant H II region N 11 (Henize 1956) or DEM 34 (Davies et al. 1976) is the second most important H α emission complex in the Large Magellanic Cloud (LMC) after the famous 30 Dor (see e.g. Rosado et al. 1996 and references therein). Interestingly, this region has been suggested to be reminiscent of an evolved, some 2×10^6 years older version of the 30 Dor starburst (Walborn & Parker 1992). The H II region N11 C (NGC 1769), lying at the eastern periphery of the bubble created by the central association LH 9 (Walborn & Parker 1992), is one of the brightest and youngest nebular components of the N 11 complex. N 11 C was studied by Heydari-Malayeri et al. (1987,

Send offprint requests to: M. Heydari-Malayeri (Mohammad.Heydari-Malayeri@obspm.fr)

* Based on observations obtained at the European Southern Observatory, La Silla, Chile

** Research Fellow FNRS (Belgium)

*** Postdoctoral Researcher FNRS (Belgium)

hereafter Paper I) regarding its physical properties (gas density, excitation, chemical abundances, extinction, etc.) as well as its stellar content. They determined the spectral types for 9 stars and gave *B* and *V* photometry for 57 stars in the region. These observations also revealed the presence of an anonymous compact cluster (hereafter labelled HNT) south-west of N 11C (Fig. 1). Moreover, they identified Wo 599, an O3–O4 V star, as the main ionizing source of N11 C, instead of the central object Sk-66°41 (HDE 268743) considered previously to be one of the most massive stars with a mass well over $120 M_{\odot}$ (Humphreys 1983).

Subsequently, on the basis of sharp images obtained in good seeing conditions and using high-resolution CCDs assisted by advanced image restoration methods, Heydari-Malayeri et al. (1988) showed that Sk-66°41 is actually a star cluster made up of at least six components, the main star having a ZAMS mass of $\sim 90 M_{\odot}$. More recently, adaptive optics observations at the ESO 3.6 m telescope resolved Sk-66°41 into a tight cluster of at least 12 components, the brightest component corresponding to a ZAMS mass of $\sim 50 M_{\odot}$ (Heydari-Malayeri & Beuzit 1994, hereafter Paper II).

The present paper is devoted to the stellar content of N11 C, which constitutes the central part of the OB association LH 13 (Lucke & Hodge 1970). We particularly focus on the two tight star clusters Sk-66°41 and HNT. Although adaptive optics observations have resolved Sk-66°41 (Paper II), we need colors, especially in the visible, for studying the properties of the individual components. With regard to HNT, no studies have previously been devoted to this cluster.

2. Observations and data reduction

2.1. Imaging and deconvolution

N11C was observed on 20 November 1997 using the ESO New Technology Telescope (NTT) equipped with the active optics Superb Seeing Imager (SUSI). The detector was a Tektronix CCD (#42) with 1024×1024 pixels of $24 \mu\text{m}$ ($0''.13$ on the sky), and the seeing varied between $0''.56$ and $1''.14$ (FWHM).

The observations were performed in the *uvby* Strömgrén photometric system using the ESO filters # 715, 716, 713, and 714 respectively. We were particularly careful to keep most of the brightest stars in the field under the detector's saturation

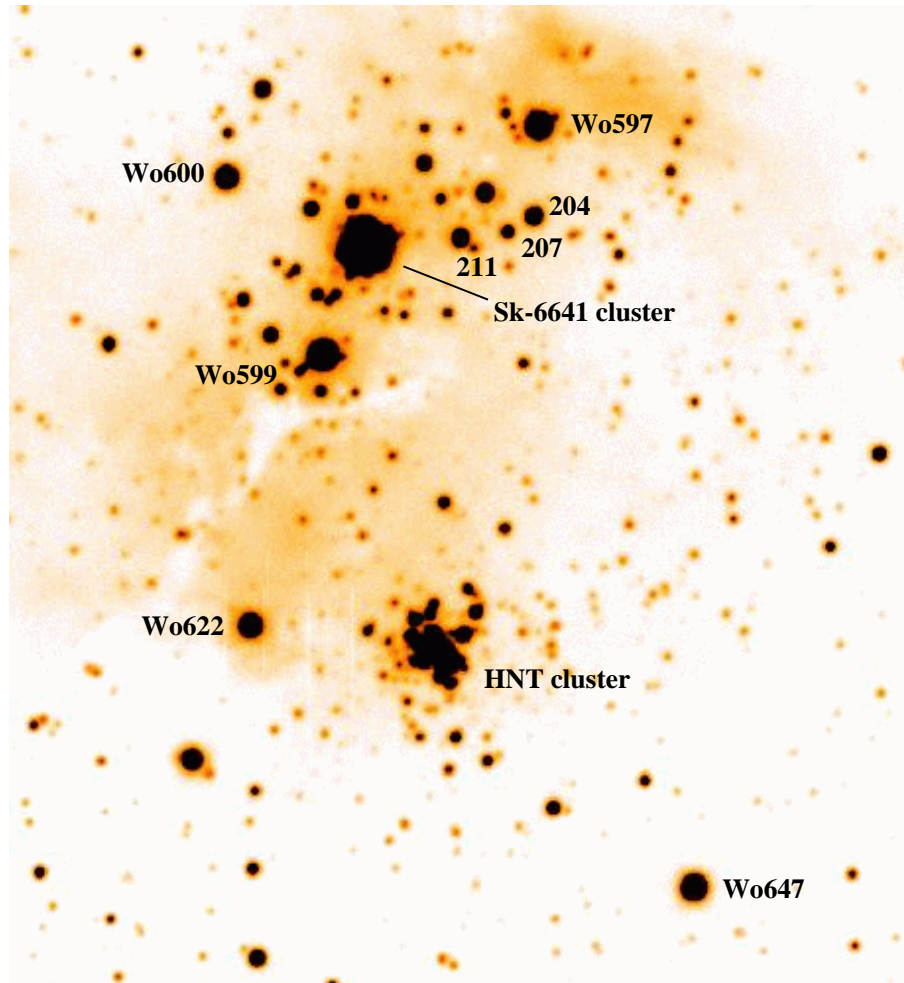


Fig. 1. The LMC H II region N11C as seen through the Strömgren b filter. The image is based on co-adding 7 dithered individual exposures. The main objects are labelled. The field size is $116'' \times 127''$, corresponding to $\sim 29 \times 32$ pc. North is up and east is left.

level to have at our disposal high quality Point Spread Function (PSF) stars. This led us to adopt exposure times of 180, 130, 150 and 90 seconds in u , v , b and y respectively. We also used ditherings of $5''$ – $10''$ for bad pixel rejection and in order to be able to use the full oversampling capabilities of the MCS deconvolution algorithm. Indeed when performing simultaneous deconvolution of several frames, the algorithm uses the different frame centerings as a constraint while decreasing the pixel size (Magain et al. 1998). We took a grid of 7 dithering positions for each filter. Luckily, the objects of interest within N11 C are close enough to hold in a single SUSI field of view. Unfortunately, the u images could not be used for the photometry due to their insufficient quality.

Photometry was derived in the Strömgren v , b and y filters according to the following procedure: after bias subtraction and flat-fielding, the seven frames were co-added in each of the filters. The photometry of the stars situated outside of the compact clusters was performed on the resulting frames through the PSF fitting algorithms ALLSTAR and DAOPHOT (Stetson 1987) implemented in the ESO MIDAS reduction package. Multiple object subtraction was performed to clean the images, but only those objects found during the first activation of the FIND sub-routine were retained for subsequent photometry. This yielded

the photometry of 344 stars lying outside the subfields of the compact clusters Sk-66°41 and HNT.

These clusters were obviously too crowded for DAOPHOT to work properly. They were instead processed with the MCS deconvolution algorithm proposed and implemented by Magain et al. (1998). The deconvolution was performed on 128×128 pixel ($16''.64 \times 16''.64$) sub-frames of the same co-added frames. Nevertheless, one of the original frames had to be removed from the sum in the y filter for cluster HNT because of a badly placed cosmic ray impact, so that only 6 frames were co-added for that filter before deconvolution of the HNT cluster. The original pixel size was reduced by a factor of two for the Sk-66°41 deconvolution but it was conserved for the restoration of the slightly less crowded HNT cluster, thus leading to final PSFs of $0''.13$ and $0''.26$ (FWHM) for the Sk-66°41 and HNT clusters respectively.

The MCS code results from a new approach to deconvolution taking care not to violate the Shannon (1949) sampling theorem: the images are deliberately not deconvolved with the observed PSF, but with a narrower function, chosen so that the final deconvolved image can be properly sampled, whatever sampling step is adopted to represent the final data. For this purpose, one chooses the final, well-sampled PSF of the decon-

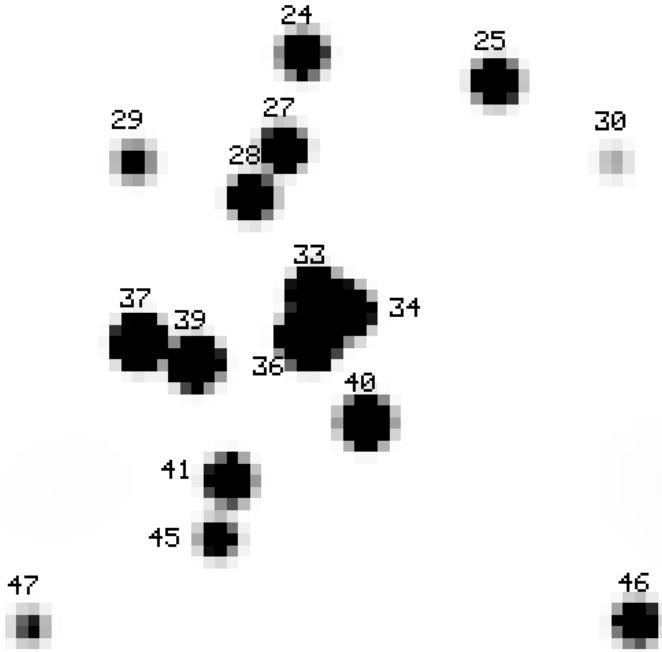


Fig. 2. Deconvolved image of the Sk-66°41 cluster, corresponding to the whole blotch appearing in Fig. 1. North is up and east is left. Field $3''.9 \times 3''.9$.

volved image and computes the PSF which should be used to perform the deconvolution. The observed PSF is constructed from several stars close enough to the clusters in order to avoid any possible PSF variation across the field.

The deconvolved frames unveil 63 and 70 objects in and around Sk-66°41 and in HNT respectively. Three of the stars in the Sk-66°41 subfield did not appear in all filters and were not included in the subsequent photometric treatment. Moreover, seven stars in HNT (#83, 86, 97, 99, 103, 113, 128) and three stars in Sk-66°41 (#18, 38, 54) were excluded from further treatment because of suspicious photometry. The omitted stars in both cases are exclusively faint components, most of which appear in or close to the densest and brightest parts of the clusters, which strongly decreases their already low intrinsic S/N. The final sample is thus made of 57 stars in the Sk-66°41 subfield and 63 in HNT.

A technical problem prevented us from using the standard star observations to calibrate the photometry. Instead we first deconvolved three bright and isolated stars in the field independently in order to fix the zero point between deconvolved and DAOPHOT photometry. Then, we fixed the y magnitudes using the V magnitudes published in Paper I: out of the 22 stars of the region around Sk-66°41 for which these authors published photometry, 14 fall into our field. The zero point in y was established by matching our instrumental y magnitudes to the published V magnitudes for 13 of them, since the fourteenth revealed a strong discrepancy with respect to the others. The result has an rms uncertainty of ± 0.12 mag. Finally, we calibrated the v and b magnitudes by making use of the three stars for which we possess both photometry and spectral type (Wo597, Wo622 and star #204), by matching their $(v - y)$ and

Table 1. Photometry of the Sk-66°41 components. To allow reference to our earlier work, the last column provides a cross-identification with the numbering adopted in Paper II.

Star	v	b	y	$b - y$	Notes
24	15.45	15.46	15.58	-0.13	#3
25	15.31	15.34	15.42	-0.08	#2
27	15.40	15.56	15.60	-0.04	#4
28	15.82	15.58	15.80	-0.21	#5
29	17.57	17.24	17.34	-0.10	#12
33	14.00	14.13	14.29	-0.15	#7
34	13.85	13.79	13.84	-0.06	#7
36	12.64	12.70	12.82	-0.12	#8
37	14.02	14.05	14.20	-0.15	#9
39	14.18	14.17	14.28	-0.11	#10
40	14.36	14.30	14.50	-0.20	#6
41	15.09	15.21	15.42	-0.21	#11
45	17.02	16.80	16.85	-0.05	#11
46	15.91	15.91	16.01	-0.11	#1
47	18.09	17.91	17.98	-0.07	

$(b - y)$ colors with those calibrated by Balona (1994) for stars with equivalent spectral types. The standard deviations of this operation are 0.03 in v and 0.01 in b .

The final photometric results for the two clusters are presented in Tables 1 and 2, while the resulting color-magnitude diagrams for the individual clusters and the field stars are shown in Fig. 4.

2.2. Spectroscopy with NTT/EMMI

The EMMI spectrograph attached to the ESO NTT telescope was used on 21 November 1997 (BLMD mode) to obtain several long slit spectra. The grating was # 12 centered on $\lambda 4350 \text{ \AA}$ and the detector was a Tektronix CCD (#31) with 1024^2 pixels of size $24 \mu\text{m}$. The range was $\lambda\lambda 3810\text{--}4740 \text{ \AA}$ and the dispersion 38 \AA mm^{-1} , giving FWHM resolutions of 2.70 ± 0.10 pixels or $2.48 \pm 0.13 \text{ \AA}$ for a $1''.0$ slit. At each position we first took a short 5 min exposure followed by one or two longer 15 min exposures. The instrument response was derived thanks to observation of the calibration stars LTT1020, LTT1788, EG21.

The seeing varied from $0''.7$ to $1''.4$. These atmospheric conditions allowed us to obtain relatively un-contaminated spectra of some of the components of the HNT cluster, but we were unable to resolve the more compact Sk-66°41 cluster spectroscopically.

3. Photometry results

3.1. Components of the clusters

Fig. 1 presents an image of N11C on which the clusters Sk-66°41 and HNT as well as the main stars are indicated. The outcomes of the deconvolution processing applied to these clusters are displayed in Figs. 2 and 3, while Tables 1 and 2 list the results of the photometry.

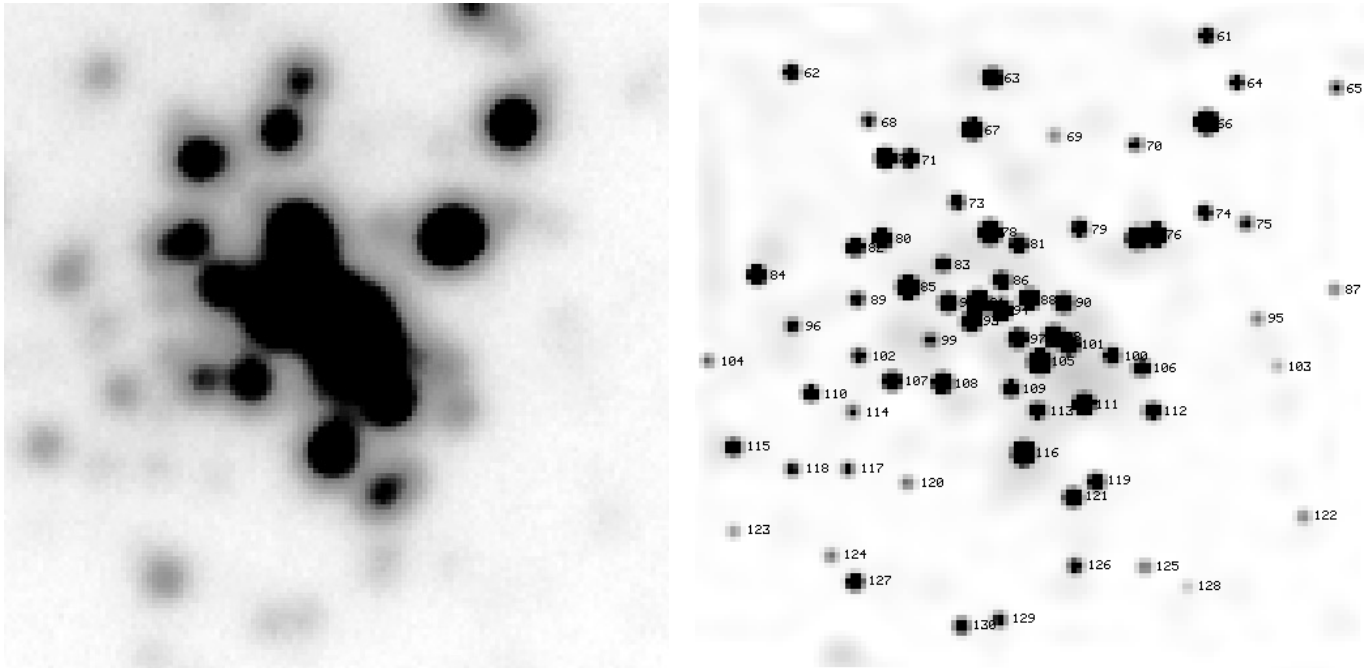


Fig. 3a and b. A close-up of the Strömgren b image (Fig. 1) focused on the HNT cluster. **a** Original image. **b** Restored image using the MCS deconvolution method. Field $16''.64 \times 16''.64$.

Table 2. Photometry of the HNT cluster

Nr.	v	b	y	$b - y$	Nr.	v	b	y	$b - y$	Nr.	v	b	y	$b - y$
61	19.77	19.52	19.72	-0.19	82	18.73	18.70	18.81	-0.11	108	17.93	17.87	17.97	-0.10
62	19.39	19.43	19.45	-0.02	84	19.24	18.27	17.70	0.57	109	19.52	19.18	19.41	-0.24
63	18.35	18.30	18.39	-0.09	85	18.03	17.13	16.56	0.57	110	19.29	19.26	19.31	-0.06
64	19.97	19.82	20.01	-0.18	87	21.31	20.93	20.36	0.57	111	17.67	17.56	17.67	-0.11
65	20.55	20.40	20.40	-0.00	88	17.85	17.74	17.81	-0.07	112	19.26	19.10	19.21	-0.11
66	17.29	16.58	16.16	0.42	89	19.96	19.84	20.11	-0.27	114	21.03	20.62	20.64	-0.02
67	17.79	17.74	17.83	-0.09	90	18.61	18.40	18.54	-0.14	115	19.56	19.44	19.53	-0.09
68	20.10	20.12	20.31	-0.19	91	16.76	16.46	16.23	0.23	116	17.49	16.81	16.44	0.37
69	21.22	21.11	21.19	-0.08	92	18.47	18.32	18.44	-0.13	117	20.56	20.40	20.36	0.03
70	20.43	20.24	20.26	-0.02	93	18.00	17.88	17.95	-0.07	118	20.53	20.32	20.25	0.07
71	19.03	18.88	19.02	-0.14	94	17.48	17.46	17.48	-0.02	119	19.17	19.00	19.07	-0.06
72	17.88	17.84	17.87	-0.03	95	21.41	21.06	20.99	0.06	120	20.92	20.83	20.86	-0.03
73	19.80	19.67	19.96	-0.29	96	20.54	20.22	20.44	-0.22	121	18.42	18.36	18.47	-0.11
74	19.81	19.66	19.74	-0.08	98	17.53	17.59	17.62	-0.03	122	21.63	21.04	20.85	0.20
75	20.59	20.40	20.50	-0.10	100	19.56	19.31	19.54	-0.23	123	21.49	21.32	21.13	0.19
76	17.64	17.57	17.67	-0.10	101	17.90	17.74	17.94	-0.20	124	21.37	20.96	20.95	0.01
77	17.43	17.36	17.44	-0.08	102	20.01	19.90	20.06	-0.17	125	20.98	20.80	20.74	0.06
78	16.92	16.88	16.94	-0.06	104	21.01	20.84	20.71	0.13	126	20.24	19.91	20.04	-0.13
79	19.55	19.37	19.51	-0.14	105	17.24	16.57	16.15	0.43	127	19.02	18.93	19.01	-0.08
80	18.18	18.10	18.19	-0.09	106	19.46	19.34	19.48	-0.14	129	20.39	20.16	20.21	-0.05
81	19.16	18.93	18.98	-0.05	107	18.49	18.42	18.54	-0.12	130	20.21	19.47	19.01	0.46

The comparison of the present results for Sk-66°41 with those obtained using an adaptive optics system (Paper II) is interesting. For this purpose, Fig. 2 has the same size as the Fig. 2 in that paper which displays a deconvolved image in the near infrared K band. The similarity is almost perfect, although the present observations reveal 15 components in Sk-66°41 instead of 12. The cross identification between the components of the

visible and infrared images is listed in Table 1. The discrepancy in the number of components is due to the fact that the images represent two distinct wavelength ranges and also the clean procedure used for the K image may be partially responsible. Anyhow, the MCS deconvolution code reveals that the core of Sk-66°41 is most probably made up of at least three components (stars #33, #34, and #36). These are all hot stars,

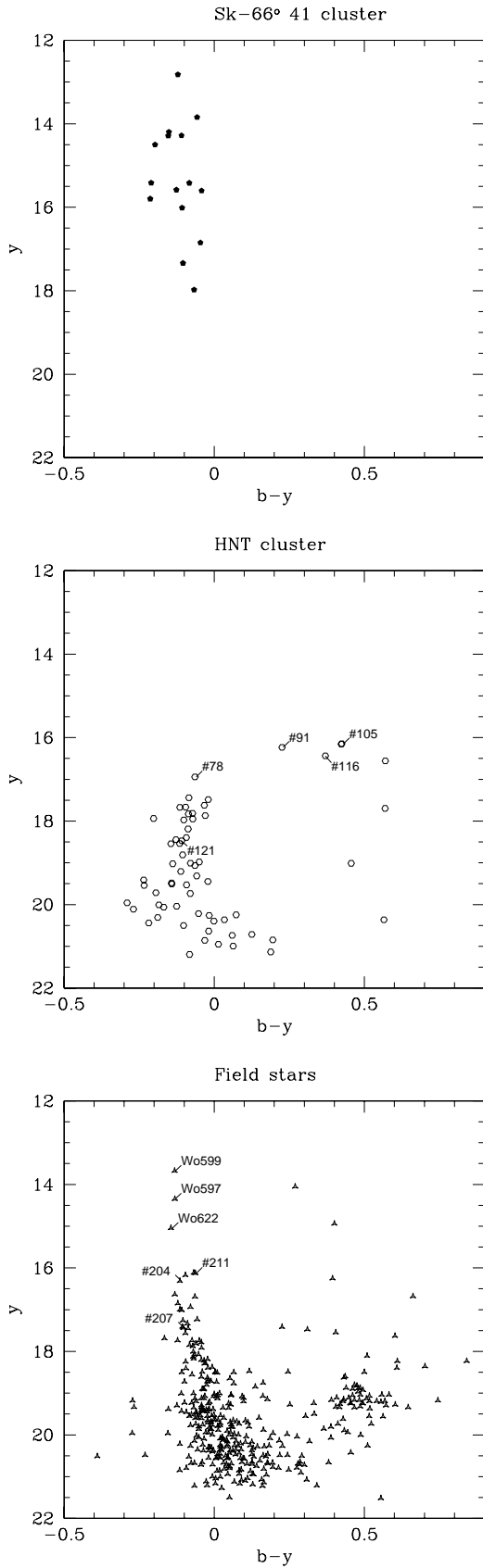


Fig. 4. Color-magnitude diagrams of the clusters, Sk-66°41 and HNT, and the field stars.

as indicated by their colors. The brightest star of the cluster is #36 with $y = 12.82$.

The HNT cluster is apparently richer than Sk-66°41 but is made up of fainter stars (Table 2, Fig. 3). Only six stars (#66, #78, #85, #91, #105, and #116) appear brighter than $y = 17$ mag. HNT is generally composed of blue stars, although apart from star #78, all of the six brightest stars have red colors.

3.2. Field stars

The two compact clusters form the densest parts of the LH 13 association (Lucke & Hodge 1970). Photometry was obtained for 344 stars within the field of LH 13 but lying outside the clusters. Several of the brightest ones were also observed spectroscopically, as presented in Sect. 4.

Of particular interest is Wo599. We applied the deconvolution technique to look into its multiplicity, since it has a composite spectrum (see Sect. 4.3). This method did not reveal any close components towards Wo599. The closest stars to Wo599, as shown by the images, are two faint stars of $y = 19.68$ and $y = 19.38$ lying at $2''.6$ west and $2''.9$ east of Wo599 respectively. This result does not, however, prove that we are dealing with a single star.

4. Spectral types

4.1. Sk-66°41 cluster

It was not possible to obtain the individual spectra of the components of Sk-66°41. Therefore the spectrum (Fig. 5) represents the whole cluster dominated by the brightest central stars (#33, #34, #36). If one were to force a single spectral type, it would be O6.5 V ((f)). However, that classification is not satisfactory, because there are opposite discrepancies. The N IV $\lambda 4058$ emission (stronger than N III $\lambda\lambda 4634-40$) and N V $\lambda 4604$ absorption show the presence of a (non-dominant) O3 component, while the weaker He I lines such as $\lambda\lambda 4009, 4144, 4387$ require a component at least as late as O8. Hence, we derive O3 V ((f*)) + OB. This result revises the previously published classification O5 V, based on lower S/N spectra (Paper I).

4.2. HNT cluster

Fig. 6 displays the spectra of some of the brightest stars in the HNT cluster. To limit the contamination by nearby fainter stars, the spectra were extracted over a rather narrow range of four pixels ($\sim 1.5''$) centered on the location of the relevant star along the slit projected on the sky. We caution however that the resulting spectra are slightly contaminated by the nearby fainter stars, especially near the crowded cluster center.

Our spectra of the brighter members of the HNT cluster correspond to stars of spectral type A-F. We have classified these spectra using the criteria described by Gray & Garrison (1987, 1989a, b). While these criteria are well established for Galactic stars, their application to stars in the LMC is more ambiguous because of the well known metal deficiency of the latter galaxy. Therefore, there is a dispersion among the classifications based

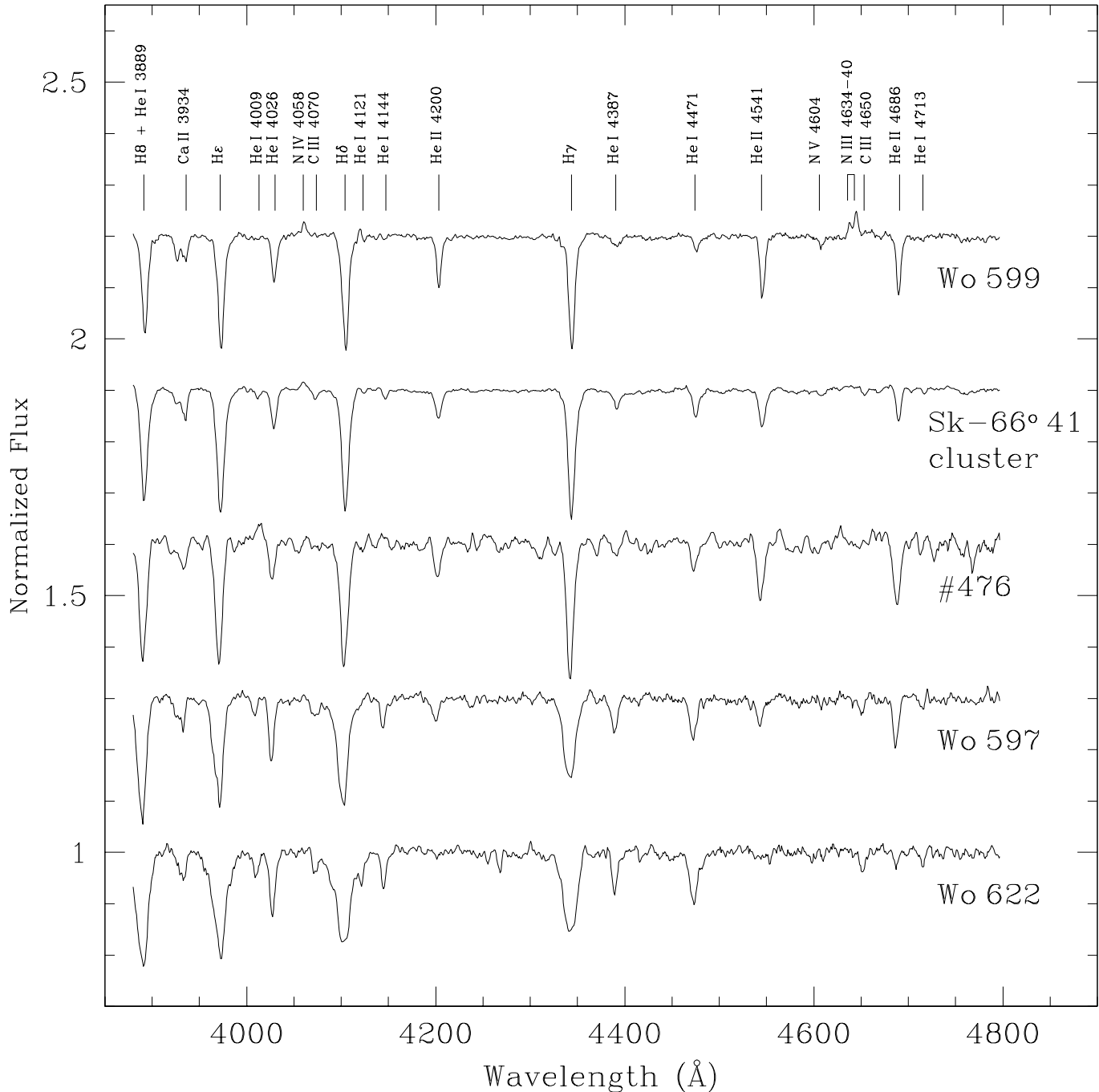


Fig. 5. Normalized spectra of the brightest O type stars towards N11 C. That of Sk-66° 41 corresponds to the whole cluster shown in Fig. 2. The spectra are shifted vertically by 0.3 units.

upon different criteria for the same star. We find that the ratio of the strength of the Ca II K line with respect to the Ca II H + He I line yields an earlier spectral type than the other criteria based for instance on the strength of the Balmer lines. Since the Ca II lines are weakened compared to Galactic standard stars, we favor the classification based on the other criteria. Table 3 lists the results for five bright stars in the HNT cluster.

The luminosity classification of A-F stars largely relies on the intensities of metal lines (e.g. Gray & Garrison 1987, 1989a,

b) and is therefore rather unreliable for the LMC stars discussed here. We emphasize however that the shape of the wings of the Balmer lines points towards a giant or even supergiant luminosity classification. Adopting a distance modulus of 18.5 and assuming an average $E(B - V) = 0.22$ mag towards N11C (Paper I), we derive the absolute visual magnitudes listed in Table 3. These values roughly correspond to luminosity class III – II. We caution however that these results might be affected by multiplicity of the stars considered here.

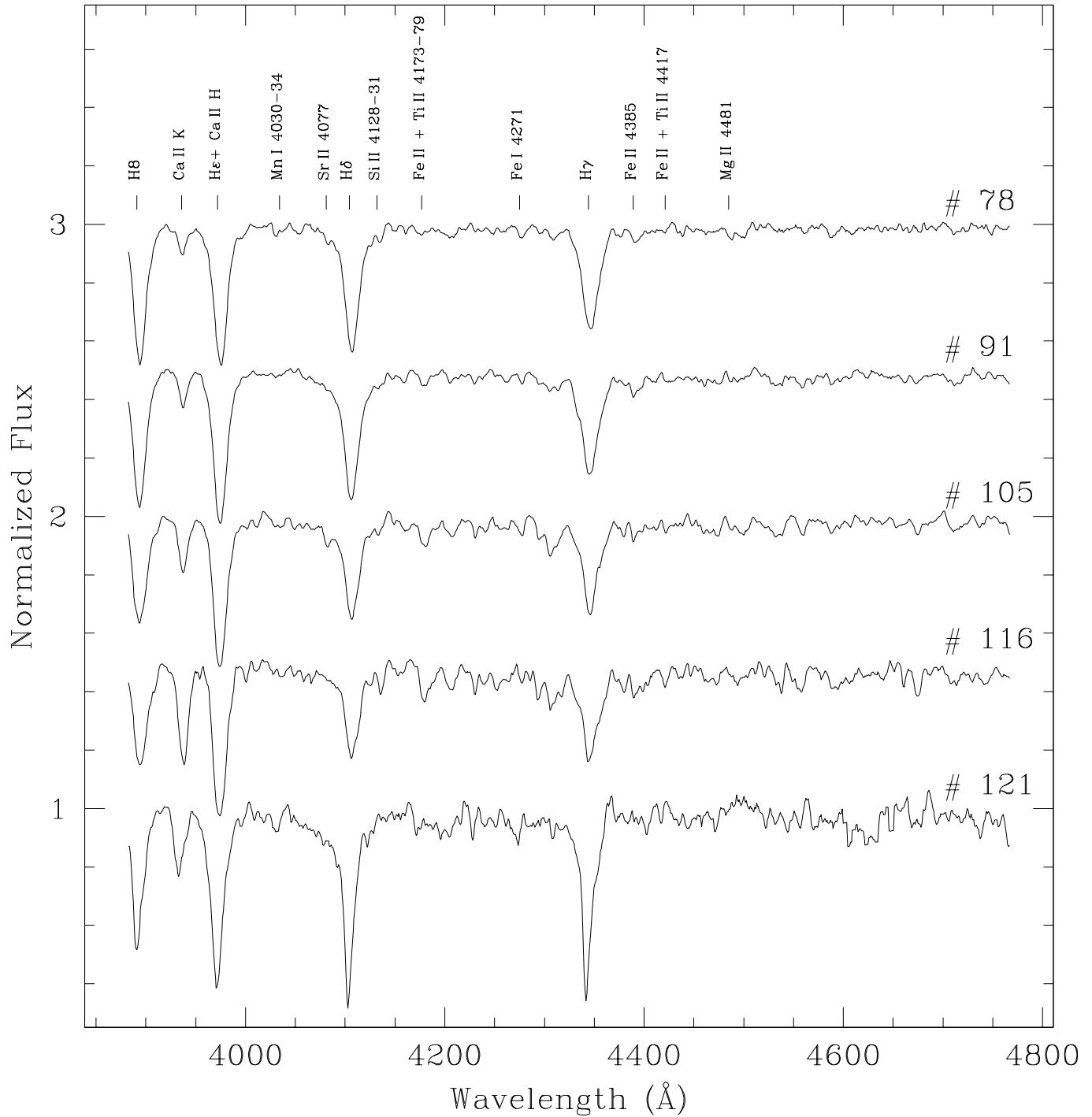


Fig. 6. Normalized spectra of five of the brightest members of the HNT cluster. The spectral features that are the most important for the classification are labelled.

We note that our spectroscopic data reveal no trace of a star earlier than A0 in the HNT cluster.

4.3. Spectral types of the field stars

A number of the field stars were studied also spectroscopically. The spectrograms of these stars are displayed in Fig. 5 and Fig. 7. Table 4 summarizes the spectral types and the measured radial

velocities. Almost all are O or B types. In the following we discuss the details of some of the individual spectra.

Wo599. This star exhibits an interesting composite spectrum. Although the N IV $\lambda 4058$ emission is prominent, it is weaker than N III $\lambda\lambda 4634-40$. The presence of C III $\lambda 4650$ emission is noteworthy. The only feature that prevents a pure O4 classification is He I $\lambda 4387$, which is somewhat strange (no other anomalously strong He I lines), and it is broader than the

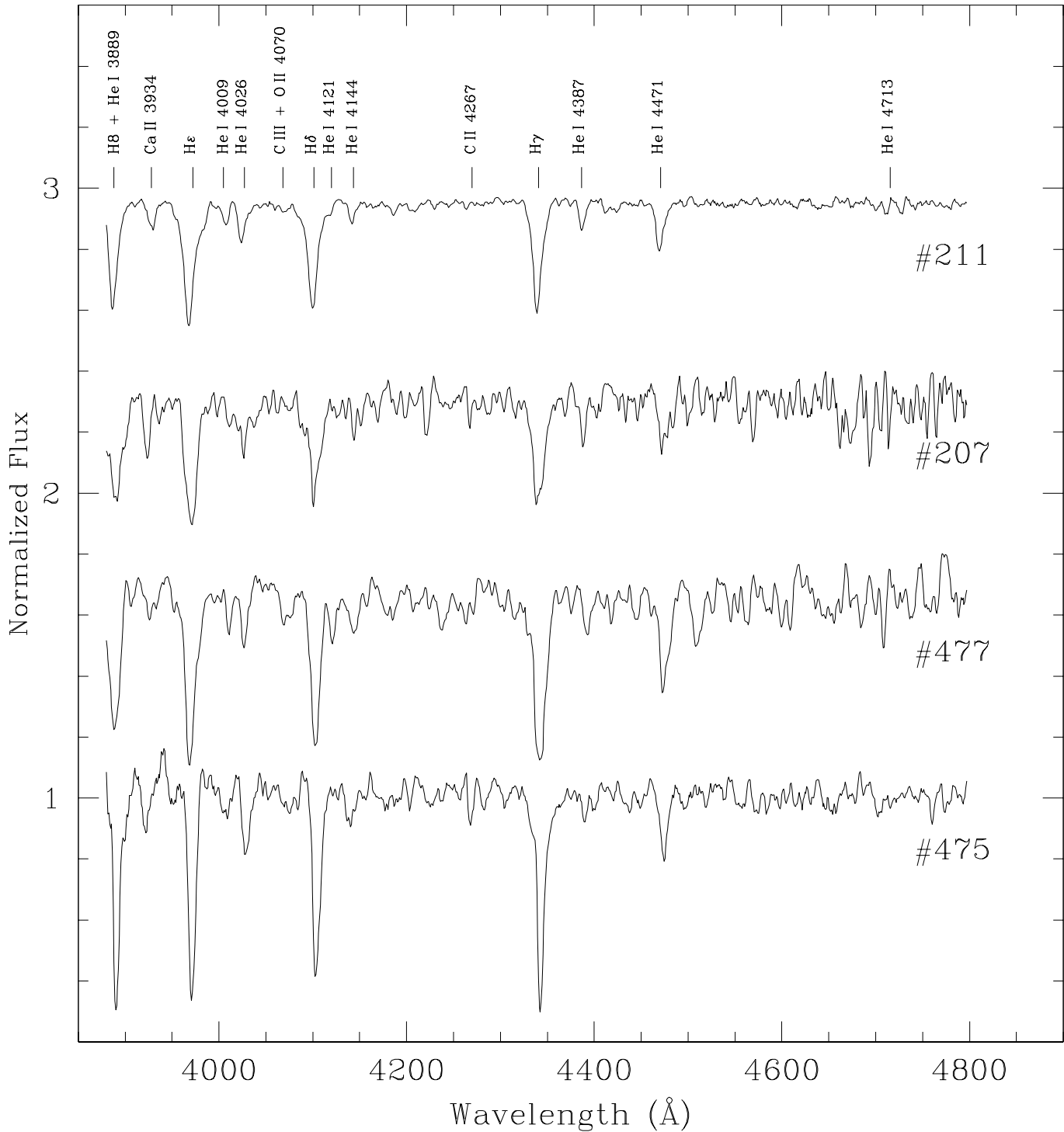


Fig. 7. Normalized spectra of B type stars towards N11 C.

other lines, which is consistent with an origin in other star(s). The required components are most probably not very late and the earlier type must dominate, otherwise He I $\lambda 4471$ would be stronger. We classify Wo599 O4 V ((f⁺))+O. The “+” tag means that the Si IV $\lambda\lambda 4089, 4116$ lines are in emission; when only the latter is visible, as in this case, it is presumed that the former is canceled by a relatively stronger absorption line.

Wo622. The classification of this star is ambiguous between O9.7 III and B0.2 V (both have He II $\lambda 4541 \sim$ Si III $\lambda 4552$). The main luminosity criterion is He II $\lambda 4686$ /He I $\lambda 4713$ and if this is a late O star, it has to be a giant from that ratio (Walborn & Fitzpatrick 1990). Should the bump at the blue edge of H δ be Si IV $\lambda 4089$, the higher luminosity class is supported, but the presence of this line is uncertain. On the other hand, if the type is

as late as B0.2 then the He II $\lambda 4686$ /He I $\lambda 4713$ ratio would be consistent with class V. Given the resolution and S/N, we cannot decide. Note however that the derived absolute magnitude (-4.1) is consistent with the later type (Vacca et al. 1996).

Star #211. The classification is B1 V, provided that a feature near He II $\lambda 4686$ is noise. If it were real, the type would have to be earlier.

Star #475. This star lies $\sim 45''$ east of Wo622 on a line joining Wo622 to the middle of HNT, outside the field of our images. Some features of the spectrum look like those of a mid- or late-B supergiant, but they are not consistent. For example, there may be strong C II $\lambda 4267$, but there is no trace of Mg II $\lambda 4481$, which should be very strong.

Star #476. This star lies $\sim 65''$ west of #204 on a line joining it to #211. It is an O6 V, assuming that a feature at $\lambda 4387$ is noise, since there are three other comparable ones near H γ . Otherwise He I $\lambda 4387$ would be too strong, but everything else is consistent.

Star #477. This star lies $\sim 46''$ east of Sk-66 $^{\circ}$ 41. Its spectral type is B0-1 V depending on the feature near He II $\lambda 4686$. If real, the earlier type applies; if not, the later.

Wo 647. We classify this star as F7-F8. Contrary to what happens for the members of the HNT cluster, the line intensities in the spectrum of Wo 647 match those of the Galactic main sequence or giant standard stars. This star has a radial velocity of $-127 \pm 11 \text{ km s}^{-1}$. Our results confirm that Wo 647 is most probably a Galactic foreground star as already suspected in Paper I.

5. Color-magnitude diagrams

We have derived color-magnitude diagrams for the two clusters and the field stars in N11C. Whilst these diagrams are solid enough for the conclusions reported in this paper, we caution that the data are not in the standard Strömrgren system.

The C-M diagram of the Sk-66 $^{\circ}$ 41 cluster (Fig. 4) displays a rather well defined main sequence in the interval $12.8 \leq y \leq 18.0$ and $-0.2 \leq b - y \leq 0.0$. There is no evidence for stars evolved off the main sequence in Sk-66 $^{\circ}$ 41.

Assuming an average reddening of $E(B-V) = 0.22$ (Paper I) and adopting a distance modulus of 18.5, we can in principle estimate the age of the various stellar populations in N11C by comparing the observed C-M diagrams with the isochrones derived from theoretical evolutionary tracks. However, fitting isochrones to very young stellar populations such as those of Sk-66 $^{\circ}$ 41 with high turn-off masses and no red supergiants is a quite difficult and rather uncertain procedure. In our case, this is even more uncertain since we are dealing with a non-standard C-M diagram. We have nevertheless attempted a comparison of our color-magnitude diagrams to the isochrones corresponding to the $Z = 0.008$ models of Schaerer et al. (1993). The isochrones were computed using a program kindly provided by Dr. G. Meynet. For the Sk-66 $^{\circ}$ 41 cluster we find that a reasonable upper limit to the age of the cluster is 5 Myr. This result is also in line with the spectral classification of the integrated spectrum of Sk-66 $^{\circ}$ 41 as O3V((f*)) + OB. In fact the most massive star

Table 3. Spectral classification and radial velocities of the stars in the HNT cluster. The radial velocities are derived from the Balmer lines excluding the He line which is heavily blended with the Ca II H line. The quoted absolute magnitudes are derived from our photometry assuming an average $E(B - V) = 0.22$ mag. The last column lists the identification of the fainter nearby stars that are likely to contribute to the spectra.

Star	Spectral type		RV km s $^{-1}$	M $_V$	Contam. sources
	Ca II	other crit.			
#78	A0 - A1		182 ± 16	-2.2	#73
#91	A0 - A2		149 ± 16	-2.9	#92, 93, 94, 86
#105	\sim A5	F0 - F3	176 ± 12	-3.0	#109
#116	late A	F3 - F5	191 ± 16	-2.7	
#121	A1 - A2	A3 - A6	160 ± 32	-0.7	#119

of the cluster has not yet left the main sequence though it shows Of emission features characterizing pre-WR stages. Assuming a lowest possible ZAMS mass of $60 M_{\odot}$ for an O3 star, this spectral type puts an upper limit on the age of this star of 3.7 Myr (Schaerer et al. 1993), in agreement with the upper limit on the cluster age derived from the C-M diagram.

The C-M diagram of the HNT cluster is also shown in Fig. 4. The labels indicate those stars for which we have derived spectral types using our spectroscopic data. The main sequence of the HNT cluster is visible up to $y \geq 17$. To the right of the main sequence, we find a couple of evolved stars with $b - y$ between 0.2 and 0.6 that are brighter than $y = 17$. Applying the same technique as above to the HNT cluster, we find from the main sequence turn-off and the red giant population that the age of this cluster is most probably 100 ± 25 Myr, i.e. much older than the age derived for the Sk-66 $^{\circ}$ 41 cluster.

The C-M diagram of the field stars in N11C is shown in Fig. 4. Inspection of this diagram reveals a mixture of stars of quite different ages. We find a main sequence that extends up to $y \sim 14.3$ as well as a couple of evolved stars to the right. Around $y = 19$ and $b - y = 0.5$, we notice the clump of older red giant field stars.

The difference in age between the two clusters is an interesting feature that raises some questions about the physical link between the HNT cluster and the N11C complex. In fact, recent studies have revealed that massive stars tend to form in a rather coeval fashion. Massey et al. (2000) report results for a sample of 19 OB associations in the Magellanic Clouds. In about half of these associations, they find that most of the massive stars formed within a short time (< 1 Myr). In the remaining associations, they found that star formation most probably occurred over a time-span of less than 10 Myr. Therefore the age difference between Sk-66 $^{\circ}$ 41 and the HNT cluster appears rather unusual if we assume that both clusters are part of the same association. The C-M diagram of the whole set of 464 stars observed towards LH 13 indicates that star formation is not coeval. This conclusion is in agreement with the results of *UBV* photometry obtained by DeGioia-Eastwood et al. (1993). A possible

Table 4. Spectral types and radial velocities of the field OB stars

Star	y	$b - y$	Velocity km s^{-1}	Type	Notes	Alternate ID
#204	16.31	-0.11	120 ± 20	O8-9: V	uncertain	#2 (Paper I)
#207	17.44	-0.10	124 ± 13	B1-2: V	uncertain	#4 (Paper I)
#211	16.13	-0.06	175 ± 38	B1 V		#1 (Paper I)
#475			160 ± 41	mid B I?	uncertain	
#476			124 ± 18	O6 V		
#477	17.36		116 ± 66	B0-1 V		
Wo597	14.35	-0.13	168 ± 30	O9 V		
Wo599	13.68	-0.14	250 ± 25	O4 V ((f ⁺)) + O		
Wo622	15.05	-0.14	227 ± 29	O9.7 III or B0.2 V		
Sk-66°41			326 ± 13	O3 V ((f [*])) + OB	cluster	

explanation could be that we are viewing different star formation regions lying at different distances along the same line of sight.

6. Discussion and concluding remarks

In this work we have obtained sub-arcsecond angular resolutions ($0''.13$ and $0''.26$ FWHM) comparable to those of the adaptive optics owing to the MCS deconvolution algorithm. This technique has allowed us to push the resolution of the Sk-66°41 cluster further into 15 components, while at the same time yielding accurate photometry of the components. It has also enabled us to present a first study of HNT, the other tight star cluster lying towards the core of the LH 13 association. With its 70 components, HNT is richer than Sk-66°41, but its stars are fainter and less massive, the brightest components being A-F types.

It is interesting to note that the *ROSAT*-HRI X-ray observations of Mac Low et al. (1998) revealed a point-like source in N 11C. Although the number of HRI counts is quite low and Mac Low et al. (1998) caution that they cannot confirm the point nature of this source, its position is in very good agreement with the optical position of the Sk-66°41 cluster. Interestingly the same HRI observations revealed no X-ray emission associated with the famous tight cluster HD 32228 at the core of LH 9 (south of N 11B) which contains at least 16 early-type stars with the brightest components being of spectral type O9 Ib and O8.5 II(f) (Walborn et al. 1999, see also Parker et al. 1992). These results suggest that the X-ray emission seen in N 11C is most probably due to the interaction of the stellar winds of the components of the Sk-66°41 cluster with the relatively dense ambient interstellar medium, whereas the lack of X-ray emission from HD 32228 is due to the lack of a sufficiently dense interstellar medium in the LH 9 region. Further constraints on the nature of this X-ray source will have to await the *XMM* observations of the N 11 complex.

The Sk-66°41 cluster harbors a very hot star of spectral type O3 and therefore provides the main exciting source of the N 11C H II region contrarily to the finding of Paper I. The ionized gas streaming from N 11C has a radial velocity of 288 km s^{-1} (Rosado et al. 1996). We have measured mean nebular line radial velocities of 296.0 and 293.6 km s^{-1} in the spectra around the

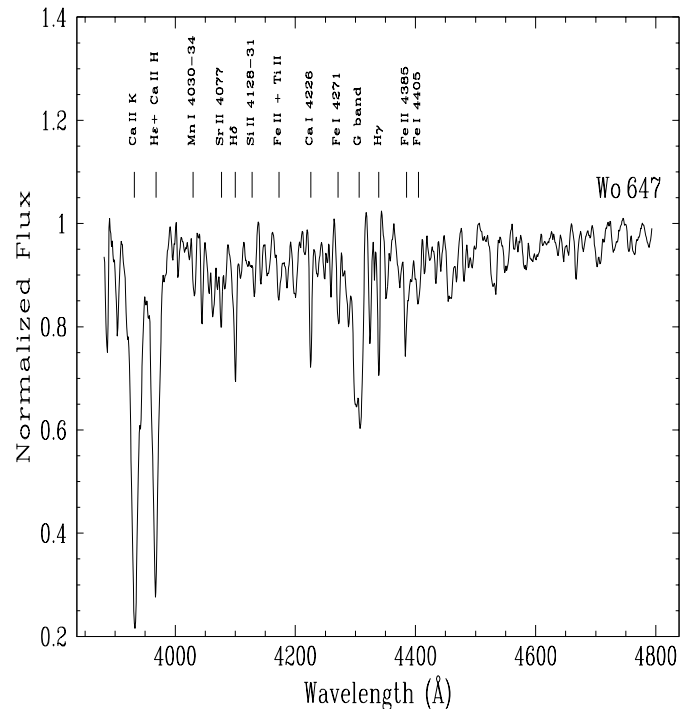


Fig. 8. Rectified spectrum of Wo 647. We classify this star as an F7 – F8 foreground star.

HNT cluster and Wo599. Given our spectral resolution, these are in very good agreement with Rosado et al.'s (1996) results.

An inevitable question is whether the two compact clusters, one high mass the other low mass, belong to the same star formation region. This question is crucial for better understanding star formation in the LMC OB association LH13. The radial velocity derived for the HNT cluster is $172 \pm 15 \text{ km s}^{-1}$ (rms), based on the five measurements listed in Table 3. Putting aside star #91, which has a somewhat discrepant velocity, yields 177 ± 11 (rms) km s^{-1} . On the other hand, the global radial velocity of the Sk-66°41 cluster is $326 \pm 13 \text{ km s}^{-1}$ (Table 4). Although it cannot be ruled out that the multiplicity and the internal motion of the stars within the Sk-66°41 cluster could alter the measured radial velocities, the velocity difference between the two clusters is probably due to their non-association.

This is in line with the drastic age difference between the two clusters (see Sect. 5).

Apart from Sk-66°41, the brightest stars towards LH 13 are Wo597, Wo599, Wo600, Wo622, and Wo647. There are two late types among them, Wo600 and Wo647, which are both Galactic F types (Sect. 4.3 and Paper I). The remaining three bright stars are O types most probably associated with LH 13 and the H II region N 11 C, although we notice that the measured radial velocities of these stars are slightly less positive than the radial velocity of the N 11 C nebular lines (288 km s^{-1} , Rosado et al. 1996) and that of the Sk-66°41 cluster. We conclude that these three stars belong to the LH 13 association as deduced from the C-M diagram. Moreover, the probability that three early type stars not belonging to LH 13 lie by chance towards this OB association should be very low. These stars have probably formed along with Sk-66°41 during the same burst.

Models studying formation of massive stars predict that these stars should never form in isolation, and that those found in isolation have been ejected from dense stellar clusters (Bonnell et al. 1998). Wo599 has a projected distance of $\sim 15''$ (3.8 pc) from Sk-66°41. Let us consider that Sk-66°41 represents the core of the massive stars resulting from the same starburst and assume that Wo599 is escaping from its birthplace. Escape velocities can be larger than 200 km s^{-1} (Leonard & Duncan 1990; Kroupa 1995), and if we arbitrarily take 50 km s^{-1} , Wo599 needs a travel time of 75 000 years to reach its present position. Wo597, would need a comparable timespan for its journey. The most distant candidate, Wo622, has a projected distance of $\sim 50''$ (12.5 pc), and requires a longer travel time of 250 000 years. These travel-time estimates are of course lower bounds, since we deal with the image on the sky of a three-dimensional configuration in space. Inversely, one can calculate the minimum velocities at which the stars could have reached their current locations. Assuming a lifetime of 3 Myr, one gets a lower velocity of $\sim 4 \text{ km s}^{-1}$ for Wo622. One might wonder whether the observed star density of the Sk-66°41 cluster is sufficiently high for the dynamical ejection mechanism to work. However, Leonard & Duncan (1988) have shown that binary-binary collisions required to produce high velocity escapees occur in low density clusters, even though simple estimates suggest that such interactions are unlikely. Furthermore, the ejection of the OB stars that we observe around Sk-66°41 must have happened during an earlier evolutionary stage when the cluster was most probably more compact than today (Portegies Zwart et al. 1999).

In summary, our high resolution images reveal two tight clusters with significantly different ages within the core of the LH 13 association. The physical connection between these two clusters is presently not clear. The younger one, Sk-66°41 (age $\leq 3.5 - 5 \text{ Myr}$) is most likely the core of a compact starburst event. The surrounding OB-stars might have been ejected from the Sk-66°41 cluster, probably as a result of dynamical inter-

action. The older cluster, HNT (age $\sim 100 \pm 25 \text{ Myr}$), contains no stars earlier than spectral types A-F and its kinematical properties as well as its color-magnitude diagram suggest that this cluster has no direct connection to the Sk-66°41 starburst and could rather be a line of sight object.

Acknowledgements. The restoration of the images to sub-arcsecond resolutions and the corresponding photometry was possible only through the use of the MCS deconvolution algorithm. We are indebted to Dr. Pierre Magain (Institut d'Astrophysique et de Géophysique de Liège, Belgium) and Dr. Frédéric Courbin (Pontificia Universidad Católica, Chile) for making the algorithm available to us and for advice. The authors express their thanks to Dr. Georges Meynet for providing the models of the Geneva group. PR and GR are greatly indebted to the Fonds National de la Recherche Scientifique (Belgium) for multiple supports. They are also supported in part by contract P4/05 "Pôle d'Attraction Interuniversitaire" (SSTC-Belgium) and by the PRODEX XMM-OM Project.

References

- Balona L.A., 1994, MNRAS 268, 119
 Bonnell I.A., Bate M.R., Zinnecker H., 1998, MNRAS 298, 93
 Davies R.D., Elliott K.H., Meaburn J., 1976, Mem. R. Astron. Soc. 81, 89
 DeGioia-Eastwood K., Meyers R.P., Jones D.P., 1993, AJ 106, 1005
 Gray R.O., Garrison R.F., 1987, ApJS 65, 581
 Gray R.O., Garrison R.F., 1989a, ApJS 69, 301
 Gray R.O., Garrison R.F., 1989b, ApJS 70, 623
 Henize K.G., 1956, ApJS 2, 315
 Heydari-Malayeri M., Niemela V., Testor G., 1987, A&A 184, 300 (Paper I)
 Heydari-Malayeri M., Magain P., Remy, M., 1988, A&A 201, L41
 Heydari-Malayeri M., Beuzit J.-L., 1994, A&A 287, L17 (Paper II)
 Humphreys R.M., 1983, ApJ 269, 335
 Kroupa P., 1995, MNRAS 277, 1522
 Leonard, P.J.T., Duncan M.J., 1988, AJ 96, 222
 Leonard, P.J.T., Duncan M.J., 1990, AJ 99, 608
 Lucke P.B., Hodge P.W., 1970, AJ 75, 171
 Mac Low M.-M., Chang T.H., Chu Y.-H., et al., 1998, ApJ 493, 260
 Magain P., Courbin F., Sohy S., 1998, ApJ 494, 472
 Massey P., Waterhouse E., DeGioia-Eastwood K., 2000, AJ 119, 2214
 Parker J.Wm., Garmany C.D., Massey P., Walborn N.R., 1992, AJ 103, 1205
 Portegies Zwart S.E., Makino J., McMillan S.L.W., Hut P., 1999, A&A 348, 117
 Rosado M., Laval A., Le Coarer E., et al., 1996, A&A 308, 588
 Schaerer D., Meynet G., Maeder A., Schaller G., 1993, A&AS 98, 523
 Shannon C.J., 1949, Proc. I. R. E. 37, 10
 Stetson P.B., 1987, PASP 99, 191
 Vacca W.D., Garmany C.D., Shull J.M., 1996, ApJ 460, 914
 Walborn N.R., Fitzpatrick E.L., 1990, PASP 102, 379
 Walborn N.R., Parker J.Wm., 1992, ApJ 399, L87
 Walborn N.R., Drissen L., Parker J.Wm., et al., 1999, AJ 118, 1684